Korean J. Chem. Eng., 34(2), 484-494 (2017)
DOI: 10.1007/s11814-016-0297-x

pISSN: 0256-1115
eISSN: 1975-7220

Synthesis of highly monodisperse silica nanoparticles in the microreactor system

Min Su†

Southwest Research & Design Institute of Chemical Industry, Chengdu 610225, Sichuan, China
(*Received 8 March 2016 • accepted 24 October 2016*)

Abstract−To avoid a poor mixing rate and local inhomogeneities in batch reactor systems, and to shorten the length of microchannels in microreactor systems, a new combined micromixer/microreactor/batch reactor system was used for the synthesis of colloidal silica particles. The silica particles with different sizes (from 20 nm to 2 μm) and size distributions (which were characterized by PDI from 0.01 to 0.40) were controllably synthesized by varying the concentration of reactants and the operating parameters in this system. The long microchannel with small diameter demonstrated a good mixing efficiency, and which produced small and uniform silica particles. In addition, the introduction of inert gas into the system intensified the mixing, and the silica particles with decreased size and narrow distribution were obtained. It was clearly demonstrated that the high mixing efficiency in the microchannel led to small and uniform silica particles. Furthermore, a theoretical foundation for the synthesis of nanoparticles in microreactors was established after illustrating the relationship of mass transfer and reaction in the system.

Keywords: Nanoparticle, Silica, Silica Nanoparticle, Microreactor, Monodispersity

INTRODUCTION

Due to chemical inertness and good biocompatibility, silica nanoparticles have attracted attentions in a wide range of potential applications in drug delivery [1,2], polymers [3], sensors [4], chromatography [5,6], catalysis [7], paints, coatings [8], adsorption [5,6] and so on. Two-dimensional ordered structures formed by these materials are potential materials for planar waveguide devices [9]. Three-dimensional structures formed by these particles have been used as templates for making ordered structures of polymers [3,10] and mesoporous carbon [11].

The Stöber method is commonly used for making silica particles [12]. Based on the hydrolysis and condensation of tetraethoxysilane (TEOS) in a mixture of alcohol, water and ammonia, the particle size and size distribution can be adjusted by changing parameters such as solvent, temperature, and concentration of ammonia, water and TEOS [12-14]. However, the silica particles obtained by this method generally have poor monodispersity and irregular shapes [15,16]. In recent years Stöber method has been modified to address this issue [17]. An alternative, widely used strategy for the synthesis of silica nanoparticles is the micro-emulsion approach, which yielded silica spheres below 50 nm diameter with superior monodispersity [18-23]. Micro-emulsion acts as a microreactor for the confined synthesis of silica nanoparticles. Due to the usage of large amounts of organic solvents and surfactants, this method has distinct disadvantages of costs and purification for industrial application. Another alternative strategy is the seeded regrowth method [24], which usually requires several days for the fabrication and thus is time-consuming. Lysine has been demonstrated to be effective for the formation of silica particles with high monodispersity due to its electrostatic interactions with silicic acid [25,26]. However, the size variation of obtained silica nanoparticles was limited to a small range [25].

Typically, the batch process is used for the fabrication of silica particles, which is simple and has the advantage of high conversions. Due to the heterogeneous distribution of reactant concentration and temperature field in the batch process resulted from insufficient mixing, it is hard to precisely control the particle size and size distribution [27]. On the contrary, the semi-batch process [28] has greater controllability over the resulting particle size, shape, and size distribution. This is due to the short nucleation time and the slow hydrolysis rate of the reaction obtained in the semi-batch process. Combining the advantages of batch and semi-batch processes, Kim et al. [29] obtained a narrower size distribution by the method of the semi-batch/batch than that by any single batch or semi-batch method. Kim et al. [29] also made a comparison among batch, semi-batch, batch/semi-batch and semi-batch/batch processes for the fabrication of silica nanoparticles, and concluded that the mixed batch/semi-batch system was the best way to produce a narrow particle-size distribution. However, the above four processes have a drawback as local inhomogeneity, which is the important factor to affect the monodispersity of silica particles. Besides, all the systems are difficult to scale up.

To overcome these disadvantages, the microreactor has been used in the synthesis of nanoparticles to bring a precise control of temperature and residence time for producing nanoparticles with high monodispersity. Due to the small channel dimensions (0.05-1.00 mm) and high surface-to-volume ratios (10,000-50,000 m^2/m^3 compared to 100 m^2/m^3 for batch reactors), microreactors have fast heat and mass transport rates [27]. Because of those advantages, microreactors have been proposed for the synthesis of various nanoparticles. Recently, the microreactor method has been reported for

†To whom correspondence should be addressed.
E-mail: sumin@haohua.chemchina.com

the preparation of silica nanoparticles [30-33]. Khan et al. [31] used single-phase laminar flow and two-phase segmented flow microfluidic synthesis to control the particle size and monodispersity, and obtained silica nanoparticles with narrow size distributions. Gutierrez et al. [32] compared the synthesis of silica nanoparticles in micromixer-microreactor and batch reactor systems, and found that the silica nanoparticles synthesized in the micromixer-microreactor system have narrower particle size distributions. He et al. [30] evaluated two microfluidic reactor configurations (laminar flow and segmented flow). Compared to the batch process, both microfluidic configurations produced particles with narrower size distributions and higher particle yields. However, there is no report regarding the relationship among the mixing, mass transfer and reaction of reactants in this microreactor system.

In micro-scale reactors, the mixer region (structure, scale and roughness) and the reaction channel (diameter, length and roughness) both affect the mixing performance. Until now, some types of mixers involving Y-shape [30], T-shape [34], swirl type [35], nozzle type [36], and central collision type [37] have been reported. These mixers produced nanoparticles with narrow size distributions. Kawasaki et al. [38] found that particle size decreased remarkably with the inner diameters of mixer decreasing. Ying et al. [39] found that the particle size and uniformity depended strongly on the velocity and residence time of reactants in channels. Until now, there are no reports about the effect of mixing efficiency of micromixer and microreactor on the size and uniformity of silica particles.

In this paper, the design, fabrication and operation of micromixer/microreactor/batch reactor (microreactor system) for controlled synthesis of silica particles based on the Stöber method are presented. The system contains three parts: micromixer, microreactor and stirred-tank reactor. Two reactor configurations were examined: single-phase laminar flow reactors (LFRs) and two-phase (gas-liquid) segmented flow reactors (SFRs). Single-phase laminar flow reactions were simply achieved by feeding the two liquid flows into the system. Two-phase (gas-liquid) segmented flow reactions were accomplished by merging inert gas and liquids in the micromixer and microreactor. Afterwards, the outlet stream of the microreactor flowed into a stirred-tank reactor for aging. First, the products of this system were compared with those of batch and semi-batch processes under the same condition. Second, the silica particles with different sizes and size distributions were obtained by changing the concentrations (TEOS, ammonia and water) and operation variables (flow rate, temperature and reaction time). Through illustrating the variation of particle size and size distribution over the above concentrations and operation variables, the best condition for the synthesis of highly monodispersed silica particles was obtained. Third, the relationship between the mixing efficiency and reaction was illustrated by changing the variables (diameter of microreactor, length of microreactor and reaction temperature). Lastly, the high mixing efficiency benefited from the reactants re-circulation within the slugs in SRFs was analyzed. Compared with the single microreactor, our system shortened the length of microchannel and therefore avoided the risk of blockage and fouling in the microchannel. Moreover, the silica nanoparticles fabricated in this system had a better homogeneity. Unlike almost all the previous studies [17,29-31,40-43], the solutions in this work were directly analyzed without further separation after the reaction. So the results can reflect the composition of the products more realistically.

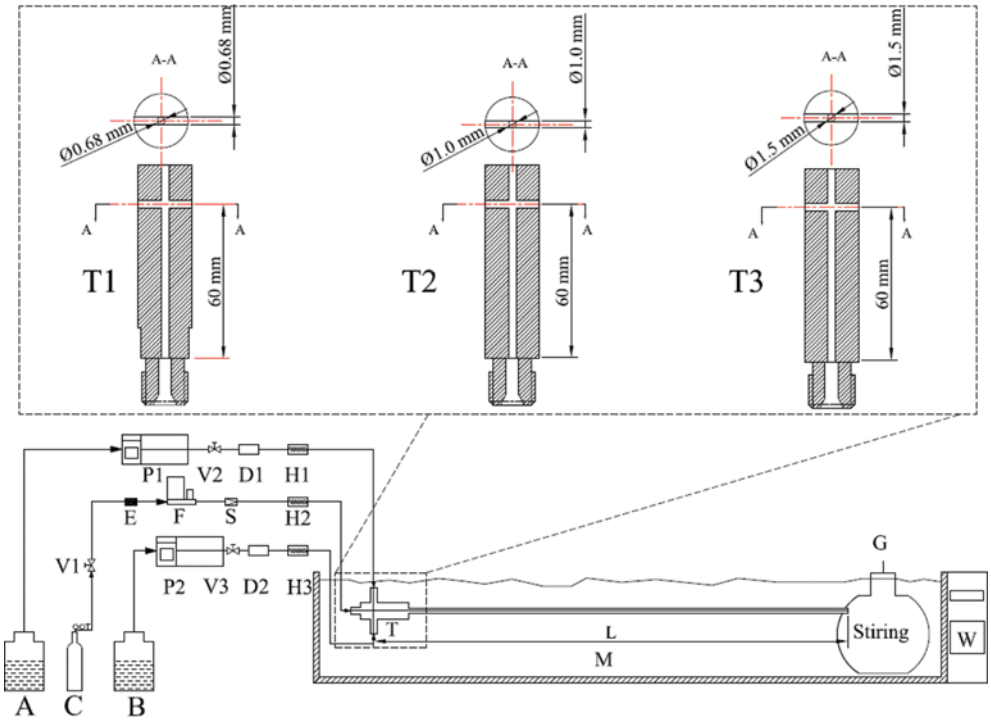

Fig. 1. Experimental apparatus of the microreactor system. (A) Ammonia solution; (B) TEOS solution; (C) Inert gas; (V1, V2, V3) Valve; (P1, P2) Pump; (D1, D2) Buffer tank; (H1, H2, H3) Heat exchanger; (F) Mass flowmeter; (S) One-way valve; (T) T-type mixer; (M) Microreactor; (G) Flask; (W) Water bath; (T1, T2, T3) micromixer with the diameter of 0.68 mm, 1.00 mm and 1.5 mm, respectively.

EXPERIMENTAL

1. Materials

Tetraethyl orthosilicate (TEOS, kermel, Tianjin), ammonium hydroxide (25 wt%, kermel, Tianjin), ethanol (kermel, Tianjin) and all other reagents were used as received, without further purification.

2. Apparatus

The experimental apparatus used for the synthesis of silica nanoparticles is shown in Fig. 1. Two micro pumps (P1 and P2, LabAlliance Series II Pump) were used to feed the solution A (a mixture of ammonia, water and ethanol) and B (containing TEOS and ethanol) into the system. Two buffer tanks (D1 and D2) were used to buffer the pulse of pumps. After that, the reactants entered the heat exchangers (H1and H2) and were heated to a pre-set temperature. Then the two streams were mixed in the micromixer. There are three different types of dimensional T-shaped mixers with the diameter (ID) of 0.68 mm, 1.00 mm and 1.50 mm, respectively, which were characterized by microscope (Olympus SZX16). The detailed diagrams of mixers used in this work are shown in Fig. 1. The glass microreactors (M) with different lengths were connected to the outlet of the mixer for further mixing and reaction. Note that the inner diameter of the microreactor was the same as that of the mixer. A flask (G) with a magnetic stirrer was used to collect the solution from the microreactor. The outlet of the microreactor and the inlet of the flask were connected by a silicone tube (ID=6 mm). Because the silicone tube was very short and the dimension was much larger than that of the mixer and microreactor, the mixing, mass transport and reaction in the silicone tube could be neglected. Two water baths were used to control the temperatures of the mixer, microreactor and flask. The segmented flow could be formed by introducing an inert gas (C) into the microreactor. The flow of the gas was controlled by a mass flowmeter (F, Sevenstar D07-11C MFC).

3. Synthesis Protocol

Solution A was fed by P1, stabilized by D1, heated by H1, flowed into T-shape mixer and mixed with solution B, which was fed by P2, stabilized by D2, and heated by H3. As for the two-phase segmented flow, the nitrogen gas (C) was controlled by a mass flowmeter, heated by H2, and used to generate small plugs within the micromixer and microreactor. Then the reaction streams mixed and reacted in the microreactor continually. Finally, the mixed solutions from the microreactor entered the flask and were aged. Different mixing effects were also accomplished by varying the inner diameter and length of the microreactor. In addition, the silica particles with different sizes and size distributions were obtained by changing the variables (diameter of microreactor, length of microreactor and reaction temperature).

In addition, the reaction conditions (concentrations of reactants, the reaction temperature, the overall reaction time, the volume of reaction solution, the stirring rate in the flask) of the three systems (microreactor, batch reactor and semi-batch reactor) were all the same as for the comparative experiments. The specific reaction conditions are presented in Table 1.

4. Characterization

Malvern Zetasizer Nano ZS90 (Malvern) instrument was used to determine the mean particle size and size distribution of obtained silica nanoparticles. The transmission electron microscopy (TEM) measurement was carried out with a FEI Tecnai G2 Spirit equipment (FEI) operated at an accelerating voltage of 120 kV. The solution after reaction was directly dropped onto a copper grid with amorphous carbon film, and then dried in air. The optical photographs of flow patterns with different gas (nitrogen)/liquid flow ratios were taken by Cannon 5D Mark II.

Table 1. Silica particles synthesized from microreactor, batch reactor and semi-batch reactor systems

Method	Mean particle size (nm)	PDI[d]	Yield[e]
Microreactor[a]	58	0.064	74%
Batch reactor[b]	18	0.227	42%
Semi-batch reactor[c]	20	0.203	19%

[a]Solution A (a mixture of ammonia, water and ethanol) and solution B (containing TEOS and ethanol) were both heated to 78 °C, flowed into T-shape mixer (ID=0.68 mm) at the same volumetric rate of 2.06 ml/min, passed through the microreactor (L=60 mm, ID=0.68 mm), then entered the flask (revolutions per minute (rpm)=300) and aged at 78 °C. The mixing direction in the T-shape micromixer (T_{MX}) was 180 °. The time of feeding solution was 60 minutes, and the aging time was 120 minutes

[b]123 ml solution A (a mixture of ammonia, water and ethanol) and 123 ml solution B (containing TEOS and ethanol) were both heated to 78 °C, quickly poured into the flask (rpm=300) simultaneously and stirred for 180 minutes

[c]Solution B (containing TEOS and ethanol) was heated to 78 °C and pumped into the flask with A (a mixture of ammonia, water and ethanol, 123 ml, 78 °C) at the volumetric rate of 2.06 ml/min, then stirred (rpm=300). The time of feeding solution was 60 minutes and the aging time was 120 minutes

[a,b,c]Silica particles were all synthesized in the three systems at the following conditions: C_{TEOS} (concentration of TEOS)=0.5 mol/L, C_{NH_4OH}=0.78 mol/L, C_{H_2O}=5.8 mol/L, temperature=78 °C, time=3 h, the volume of reaction solution=246 ml

[d]Polydispersity index (PDI) is automatically calculated by the system software from the cumulant analysis as defined in ISO 13321 : 1996

[e]Yield=(the weight of silica particles obtained from the colloidal silica solution)/(the calculated weight of silica particles from the TEOS entered the reaction system)

RESULTS AND DISCUSSION

1. Comparison of Silica Particles Synthesized from Microreactor, Batch Reactor and Semi-batch Reactor Systems

Table 1 and Fig. 2 represent the particle size, polydispersity index (PDI) and yield of silica nanoparticles obtained from microreactor, batch reactor and semi-batch reactor systems. To compare the performance of three different systems, the same reaction time (3 hours) and reaction solutions volume (246 ml) were controlled. It was found that the mean particle size and yield of the microreactor system were 58 nm and 74%, respectively, which were larger than other two systems. In the microreactor system, the reactants reacted before entering the flask, so that the TEOS evaporation was

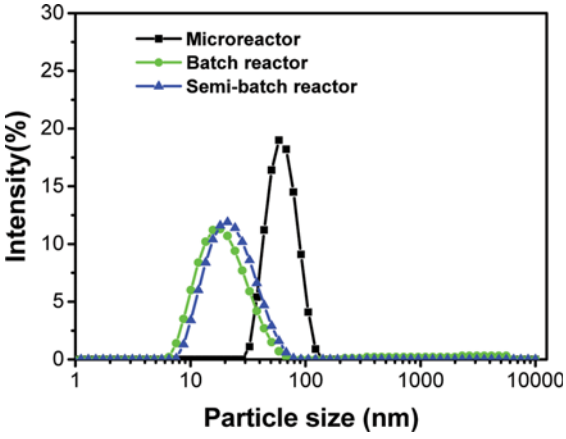

Fig. 2. The size distribution of silica particles synthesized in the microreactor, batch reactor and semi-batch reactor systems.

less than other two systems. Due to the excellent mass transfer and mixing efficiency in the microreactor, the time of nucleation was shortened. Besides, the silica monomers (which were produced afterwards and did not form silica nuclei in the microreactor and flask) were added to the surface of silica synthesized previously, and then the nuclei would grow. Thus, the particle size of silica obtained in the microreactor system was the largest one among three systems. However, a homogeneous reaction environment was formed in the microreactor system, which results in a uniform particle size. As for the semi-batch reactor system, the slow feeding rate of solution A (TEOS) led to more evaporation of TEOS than that of batch reactor, and then the yield was less than that of batch reactor. However, a relatively long growth time of silica particles occurred during the semi-batch process, which resulted in larger silica particles with narrower particle size distribution than that of batch reactor [29]. Above all, the PDI value and yield of silica par-

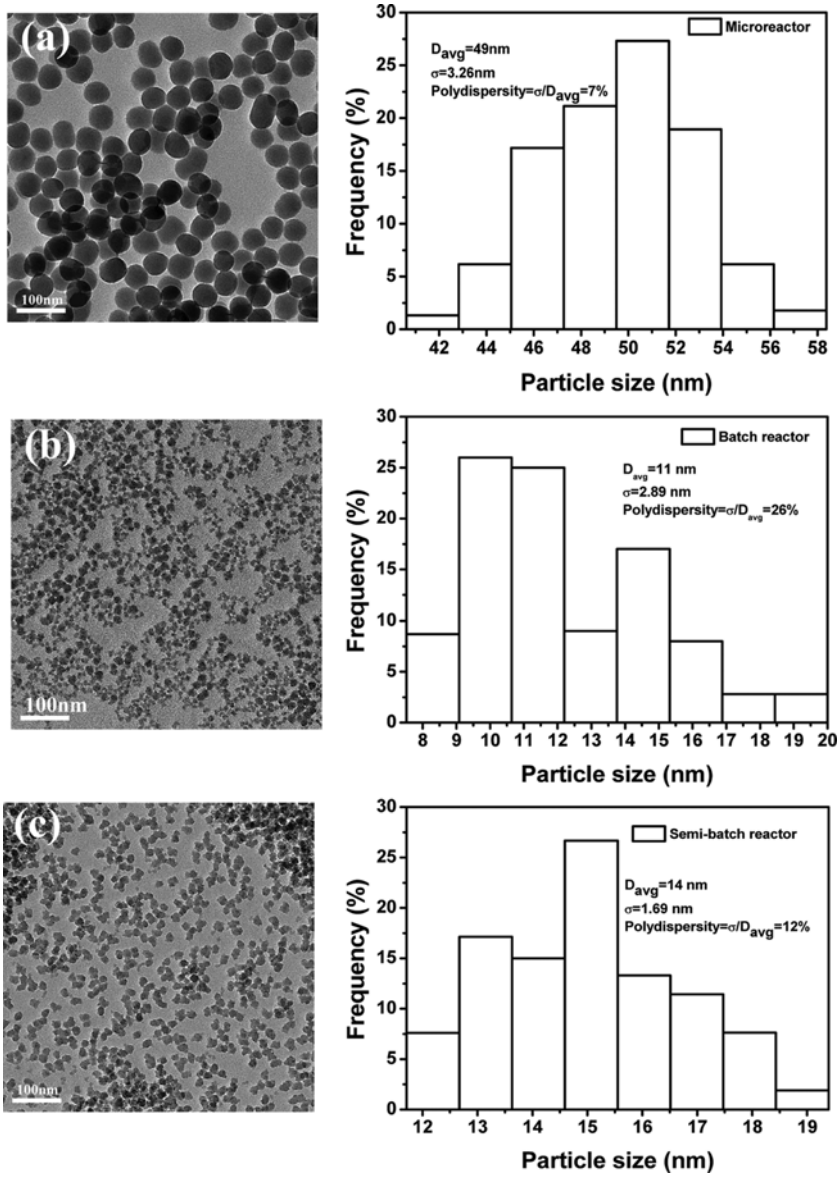

Fig. 3. TEM images of silica particles synthesized in microreactor (a), batch reactor (b) and semi-batch reactor (c) systems.

ticles synthesized in the microreactor system were better than other two systems, which showed a great advantage for the synthesis of silica nanoparticles.

The dynamic light scattering (DLS) results (Table 1 and Fig. 2) were confirmed by the TEM images (Fig. 3) of the silica particles synthesized in the three systems. As depicted in Fig. 3, the results of TEM images were close to those of the DLS.

2. Effect of the Concentration of TEOS, H_2O and NH_4OH

Silica formation involves two separate steps: hydrolysis and condensation of TEOS. Three reactions [5] are generally used to describe the two steps:

$$\equiv Si-OR+H_2O \underset{\text{Esterification}}{\overset{\text{Hydrolysis}}{\rightleftharpoons}} \equiv Si-OH+ROH \quad (1)$$

$$\equiv Si-OR+\equiv Si-OH \underset{\text{Alcoholysis}}{\overset{\text{Alcohol condensation}}{\rightleftharpoons}} \equiv Si-O-Si+ROH \quad (2)$$

$$\equiv Si-OH+\equiv Si-OH \underset{\text{Hydrolysis}}{\overset{\text{Water condensation}}{\rightleftharpoons}} \equiv Si-O-Si+H_2O \quad (3)$$

where R is an alkyl group C_2H_5. In the hydrolysis reaction (Eq. (1)), TEOS is hydrolyzed to produce siloxane molecules and ethanol. Then the siloxane molecules condense with TEOS molecules releasing ethanol (Eq. (2)) or with themselves releasing water (Eq. (3)). All the three reactions are reversible [44]. Park et al. [13] found that high concentrations of ammonia and water could accelerate the hydrolysis reaction rate. During the induction time, the TEOS molecules continuously formed the hydrolyzed monomers [45]. The monomers were partially hydrolyzed species [46]. The nucleation begins when the monomer concentration is higher than a critical value [47,48]. Once the monomer concentration decreases below the concentration of nucleation, the nucleation stops [17]. However, the monomer will also react with the surface of nuclei until the monomer concentration drops below the concentration of solubility. This process leads to the growth of the particles [13]. LaMer and Dinegar [49] proposed that the nucleation occurs within a finite period of time, and then the particles will grow through a self-sharpening mechanism. The short nucleation process is known to be essential for the synthesis of uniform silica particles with the Stöber method [13,29]. According to the theory of "nucleation burst," the synthesis of uniform particles requires that all nuclei are produced at the same time to ensure identical growth histories [47, 49,50]. As for the long nucleation phase, the particle size differs largely because the nuclei are produced at different times and the growth histories are different [47,49]. Additionally, the homogeneous concentration environment in the micromixer and microreactor would result in uniform particles.

Fig. 4(a) represents the effect of TEOS concentration on the mean size and PDI value of silica nanoparticles in the microreactor system. The average particle size increased with the concentration of TEOS increasing. This trend agreed with the results of Vasconcelos et al. [51]. Furthermore, the PDI value of the silica nanoparticles decreased from 0.25 to 0.13 at the TEOS concentration of 0.5 mol/L, and then almost remained at 0.13 when the TEOS concentration ranged from 0.5 mol/L to 1.0 mol/L. At higher TEOS concentrations, more monomers were produced from TEOS, so

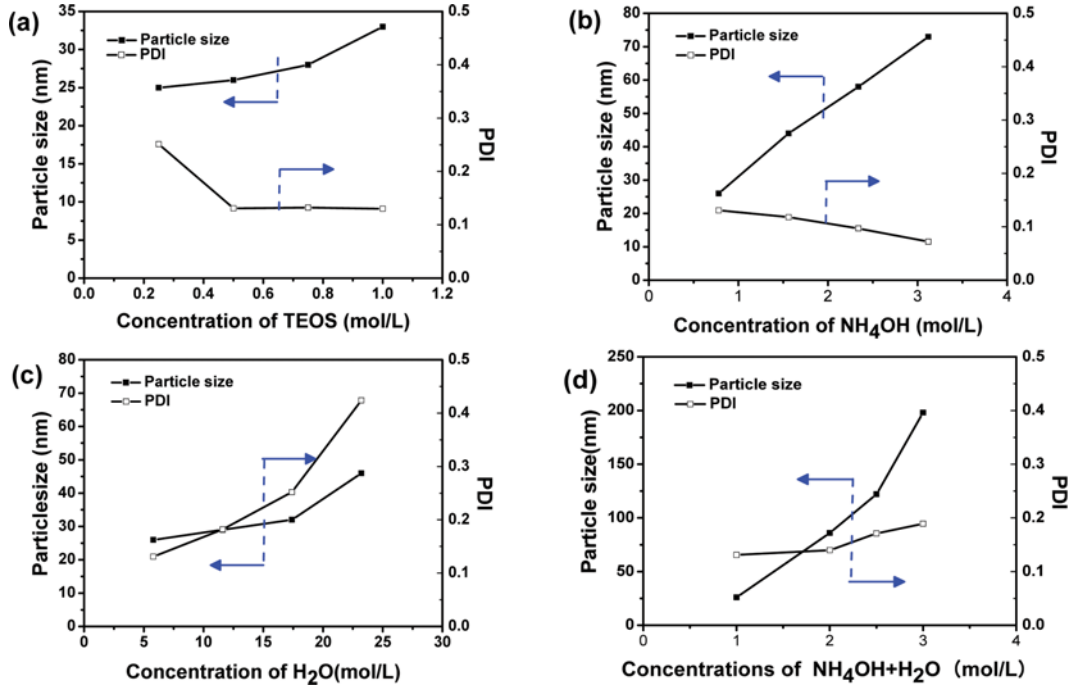

Fig. 4. The effect of (a) TEOS, (b) NH_4OH, (c) H_2O and (d) NH_4OH+H_2O on particle size and PDI: (a) C_{NH_4OH}=0.78 mol/L, C_{H_2O}=5.8 mol/L; (b) C_{TEOS}=0.5 mol/L, C_{H_2O}=5.8 mol/L; (c) C_{TEOS}=0.5 mol/L, C_{NH_4OH}=0.78 mol/L; (d) C_{TEOS}=0.5 mol/L, X=1 (C_{NH_4OH}=0.78 mol/L, C_{H_2O}=5.8 mol/L). Reaction condition: T_{MX}=180°, L=60 mm, ID=0.68 mm, V_A (flow rate)=V_B=0.057 m/s, temperature=80 °C, time=1 h/2 h (feeding time of solutions=1 h, aging time=2 h).

the time of monomer reaching the nucleation concentration was shortened and more nuclei were formed within the short time scale. Therefore, more uniform particles were formed at higher TEOS concentrations. The PDI value decreased as the TEOS concentration increased from 0.25 mol/L to 0.5 mol/L. The number of nuclei formed per total silica amount during the nucleation burst increased with the TEOS concentration increasing. However, as the TEOS concentration increased from 0.5 mol/L to 1.0 mol/L, the number of nuclei formed per total silica amount during nucleation burst was almost the same. Thus, the PDI remained almost constant. Hence, the concentration of TEOS was set at 0.5 mol/L in the subsequent experiment.

Fig. 4(b) shows the effect of ammonia concentration on the mean size and PDI value of silica nanoparticles in the microreactor system. The average particle size increased with the NH_4OH concentration increasing. This trend agreed with the results of the batch reactor [12,17,29,43,52] and microreactor [32] system. Ammonia not only promoted the hydrolysis and polymerization rates [42], but also promoted the aggregation of nuclei [13,53]. Then the decreased particle number led to large particles. However, the PDI value decreased with the ammonia concentration increasing, which contradicted with the batch reactor results [12,13,29]. Because the mass transfer and mixing effect was increased in the microreactor system, the high ammonia concentration accelerated the hydrolysis reaction. And the shortened nucleation time resulted in uniform particles in the microreactor system. However, the local concentration gradient and inhomogeneity was large at the high concentration in batch reactor. Therefore, the uniformity of particles synthesized in batch reactor decreased with the ammonia concentration increasing.

Fig. 4(c) represents the effect of water concentration on the size and PDI value of silica nanoparticles in the microreactor system. The average particle size increased with the water concentration increasing. This trend agreed with the results of batch reactor [12, 17,29,43,52] and microreactor [32] system. The hydrogen bond of silica nuclei was stronger because of the excess water [29], which resulted in larger particles [53]. Besides, the PDI value increased with the water concentration increasing, which was in accordance with the batch reactor results [12,13,29]. Due to the stronger hydrogen bond of silica at the higher water concentration, the more random aggregation of sub-particles resulted in a more broadened size distribution. As we all know, ethanol is used to disperse the synthesized silica particles in the Stöber process. And more agglomerates of particles could be obtained at the higher water concentration.

To verify the above results, the impact of both ammonia and water on the particle size and size distribution was also investigated simultaneously. The results are shown in Fig. 4(d). The average particle size increased with the ammonia concentration and water concentration increasing. This was in accordance with the results of the batch reactor [12,17,29,43,52] and microreactor [32] system. The average particle size was 198 nm at the ammonia concentration of 2.34 mol/L and water concentration of 17.4 mol/L. And it was larger than that at the ammonia concentration of 2.34 mol/L or water concentration of 17.4 mol/L, which was due to the combined effects of both ammonia and water. In addition, the PDI value increased with the ammonia concentration and water concentration increasing. It indicated that the effect of sub-particles aggregation on the PDI value outweighed the increased mass transfer and mixing effect in the microreactor at high concentrations of both ammonia and water. Besides, as the ammonia concentration exceeded 2.73 mol/L and the water concentration exceeded 20.3 mol/L simultaneously, the silica particles aggregated at the outlet of microreactor and clogged the microchannel. It was demonstrated that there was a great aggregation of particles in the solution.

As is evidence of the results described above, changing one concentration of the reactants resulted in an improvement of one particle characteristic, while inducing deleterious effects on another particle characteristic. Therefore, based on the design and operation of microreactor system, the relationship among the mass transfer, mixing efficiency and reaction was studied in the next part to develop a robust and versatile protocol for the synthesis of silica particles in a wide range with high monodispersity.

3. Effect of Flow Rate

It is well known that the mixing efficiency is affected by the flow rate in the microreactor [31]. To eliminate the influences of residence time and diameter of microreactor, a micromixer with a constant diameter of 0.68 mm was used, and then the consistency of residence time for each superficial flow rate was obtained by changing the channel length of microreactor. As depicted in Fig. 5, the mean particle size increased with the superficial flow rate of solutions A and B increasing. In this microreactor system, the reaction in the flask had a great effect on the growth of silica particles. The increased amount of TEOS at the high superficial flow rate resulted in large silica particles. Being the same as the semi-batch process, the slow feeding of reactants into the flask was not sufficiently supplied to keep the concentration of monomers above the minimum critical supersaturation [29,54]. Finally, the monomers mainly contacted the surfaces of nuclei without forming new nuclei. Besides, the PDI value decreased from 0.22 to 0.08 as the flow rate increased from 0.038 m/s to 0.094 m/s. The higher superficial flow rate meant a higher energy and mixing intensity. Thus, the silica particles obtained at high superficial flow rate had a low

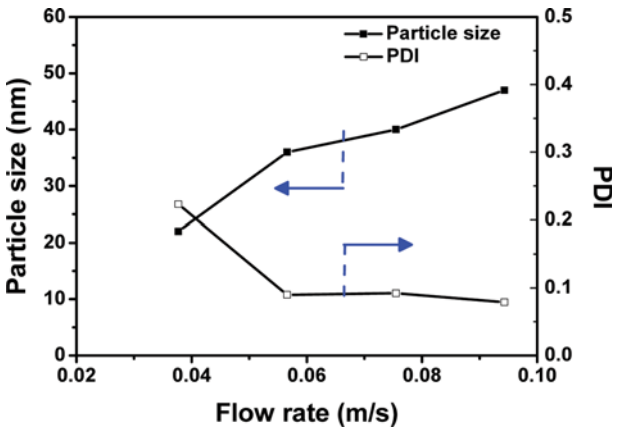

Fig. 5. The mean particle sizes and PDI values of silica nanoparticles synthesized at different superficial flow rates: C_{TEOS}=0.5 mol/L, C_{NH_4OH}=0.78 mol/L, C_{H_2O}=5.8 mol/L, T_{MX}=180°, ID=0.68 mm, L=60 mm, temperature=80 °C, time=1 h/2 h, residence time (τ)=0.8 s.

PDI value. In addition, the time needed for the nucleation of monomers was shortened. Then more nuclei formed during the nucleation leading to more uniform particle sizes [17].

4. Effect of Temperature and Reaction Time

In addition to the ammonia concentration, another important factor that affects the particle size of silica is the temperature. If the reaction temperature increases, the rate of hydrolysis and condensation kinetics (Eq. (1), Eq. (2) and Eq. (3)) will increase [17]. Due to the increase of nucleation rate, a large number of nuclei results in small particle size. The equilibrium solubility of monomers as the intermediate products obtained by the hydrolysis of TEOS increases with the reaction temperature increasing [29]. The growth of particles proceeds until the reaction stops at the equilibrium solubility of monomers. Thus, the time for the growth of particles is shortened by the increase of equilibrium solubility. Above all, the particle size of silica is reduced at a high reaction temperature. In this experiment, four temperatures (40 °C, 60 °C, 75 °C and 80 °C) were tested. Above 78 °C, most solvent was volatized into gas phase, so the critical temperature was chosen as 75 °C. To illustrate the relationship between the particle size of silica and the growth time, a total reaction time of six hours was selected. And during the reaction time, the raw materials were fed into the micromixer/microreactor and the flask continuously. After six hours, the pumps were stopped, and then the reaction solution was aged for two hours. The samples of solutions taken at different time point (1 h, 2 h, 3 h, 4 h, 5 h and 6 h) were aged for another two hours as the aging treatment.

Fig. 6(a) shows the particle size of silica with aging treatment synthesized as a function of reaction temperature and reaction time. As depicted, the particle size of silica obtained at all the four temperature points grew with reaction time increasing. And the particle size was also almost double at the eighth hour as the one at first hour. It was obvious that the particle size increased with the reaction time in a linear curve, and the slope was 112 nm/h, 21.9 nm/h, 5.97 nm/h, and 3.46 nm/h, respectively.

The synthesis of monodisperse particles was based on a uniform concentration of the reactants provided by the microchannel. In the microreactor system, a small part of the silica precursor reacted in the microchannel before entering the flask. And the other part of the silica precursor reacted in the flask during the aging process. The effect of aging treatment was to make sure the reaction was completed. The monomer and silica nuclei were both formed in the micromixer/microreactor and flask. The silica precursor previously entered the reaction vessel through the microchannel formed the silica nuclei and nanoparticles. Afterwards, the subsequent silica precursor unreacted in the microchannel entered into the flask, attached onto the surface of the nuclei and nanoparticles formed previously, which was called the secondary growth [52] of nanoparticles. Therefore, the aging process will further increase the particle size. However, not all the silica precursor attached onto the surface of the nuclei and nanoparticles formed previously. The subsequent silica nuclei were continuously formed in the micromixer, microreactor and flask during the entire reaction process, which led to the increase of particle number. As the reaction temperature increased, more silica nuclei and particles were formed due to the higher reaction rate. Thus, as for a certain amount of silica precursor, more silica nuclei and particles meant smaller amounts of silica monomers attached onto their surfaces. So it resulted in the smaller slope of the growth curve. Besides, a large amount of TEOS was consumed in the microchannel due to the increased reaction rate caused by the high reaction temperature. Therefore, the particle size of silica in the subsequent aging reaction changed a little at high reaction temperature due to the small amount of unreacted TEOS. During the subsequent aging process in the flask, the remaining TEOS reacted and then attached onto the surface of the small particles. The growth and aggregation were easier for smaller particles due to their relatively higher specific surface area. Then the aging treatment resulted in a small PDI value of silica particles. However, the PDI value of silica synthesized at 40 °C increased with the reaction time, and aging treatment was caused by a slow reaction rate at 40 °C. The continuous formation of silica nuclei and particles in the subsequent aging process led to the increased PDI value at 40 °C.

Therefore, the reaction time, aging process and the reaction temperature were the important parameters to synthesize the silica particles with the high monodispersity.

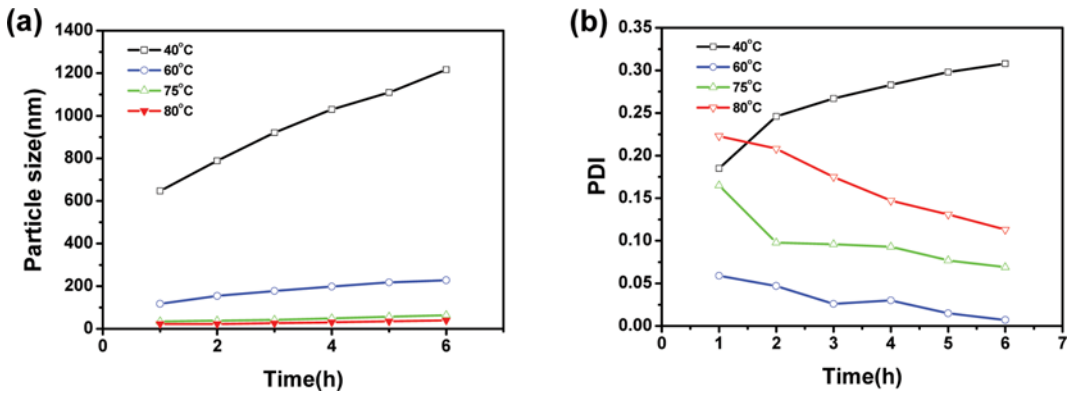

Fig. 6. Variations of particle size and PDI of silica with the time and temperature: (a) Particle size of silica at different feeding time with aging treatment of 2 hours; (b) PDI of silica at different feeding time with aging treatment of 2 hours; reaction condition: T_{MX}=180°, L=60 mm, ID=0.68 mm, V_A=V_B=0.038 m/s, C_{TEOS}=0.5 mol/L, C_{NH_4OH}=0.78 mol/L, C_{H_2O}=5.8 mol/L. The overall feeding time was 6 hours (0-6 h); and the aging time was 2 hours (6-8 h).

5. Effect of Channel Diameter and Channel Length

In microchannels, the flow pattern of a fluid is dominated by laminar flow; thus the mass transfer rate is mainly determined by molecular diffusion [55]. Diffusive mixing efficiency is usually expressed by using the Fourier number signed as Fo (Eq. (4)) [56]. Fo>0.1 indicates the system achieve a good mixing effect, and Fo>1.0 indicates it is completely mixed.

$$Fo=D_{AB}\, t/l^2 \tag{4}$$

where t is the contact time, D_{AB} is the diffusion coefficient, and l is the characteristic scale of diffusion.

As can be seen in Eq. (4), with the same diffusion coefficient, the mixing efficiency is proportional to the residence time, and inversely proportional to the square of characteristic scale (the ID in this work). Therefore, the length and diameter of microchannel has a critical influence on the mixing efficiency. In this work, four different length dimensions (60 mm, 160 mm, 360 mm and 560 mm), three different diameters (0.68 mm, 1.0 mm and 1.5 mm), and three different temperature (60 °C, 75 °C and 80 °C) were chosen to study the effect of mixing efficiency on the size and uniformity of silica nanoparticles synthesized.

Fig. 7(a), 7(c) and 7(e) represent the effects of channel length and reaction temperature on the sizes of silica nanoparticles with the channel diameter of 1.5 mm, 1.0 mm and 0.68 mm, respectively. As the channel length increased from 60 mm to 560 mm, the average size of silica particles almost all decreased. As can be seen from Fig. 7(a), the average particle size decreased greatly as the channel length increased from 160 mm to 360 mm at the temperature of 75 °C and 80 °C. In Fig. 7(c), the size of silica nanoparticles gradually decreased with the microchannel length increasing. In Fig. 7(e), the size of silica nanoparticles gradually decreased with the microchannel length increasing at 60 °C and 75 °C. For the longer microchannel reactor, the reactants were well mixed and the reactants were segmented by the solvent into small units due to the larger contact time (t as seen in Eq. (4)). Then a large amount of uniform silica particles was formed in the subsequent reaction process. In addition, more nuclei were generated in the process due to more reacted silica precursor in the mixing process, which also led to the smaller particle size. However, there were two exceptions as seen in Fig. 7. The size of silica particles (60 °C, 1.5 mm ID; 80 °C, 0.68 mm ID) almost remained unchanged with the microchannel length increasing. Because, the reaction rate at 60 °C was low and the mixing effect in the 560 mm length microchannel was non-obvious. As can be calculated from Eq. (4) (D_{AB} was calculated from the Laddha-Smith equation [57] where A was ammonia or water and B was ethanol), the Fo number (T=40 °C, ID=1.50 mm) was 0.013 even at the microchannel length of 560 mm, which indicated a poor mixing effect in the system. The particle size of silica obtained at 80 °C in 0.68 mm ID microchannel remained almost the same with the microchannel length from 60 mm to 560 mm. It can be explained that the reactants had already been mixed well at the length of 60 mm, and longer microchannel had less effect on the mixing efficiency. As can be calculated from Eq. (4) (D_{AB} was calculated from the Othmer-Chen equation [58] where A was ammonia or water and B was ethanol), the Fo number (T=80 °C, ID=0.68 mm) ranged from 0.45 to 4.2 when the microchannel length increased from 60 mm to 560 mm, which indicated good mixing had been achieved even at the length of 60 mm.

As seen in Fig. 7(a), 7(c) and 7(e), the average particle size of silica synthesized in different microchannel diameters (while the reaction temperature and microchannel were the same) was in the order of 1.50 mm>1.00 mm>0.68 mm. A better mixing effect could be

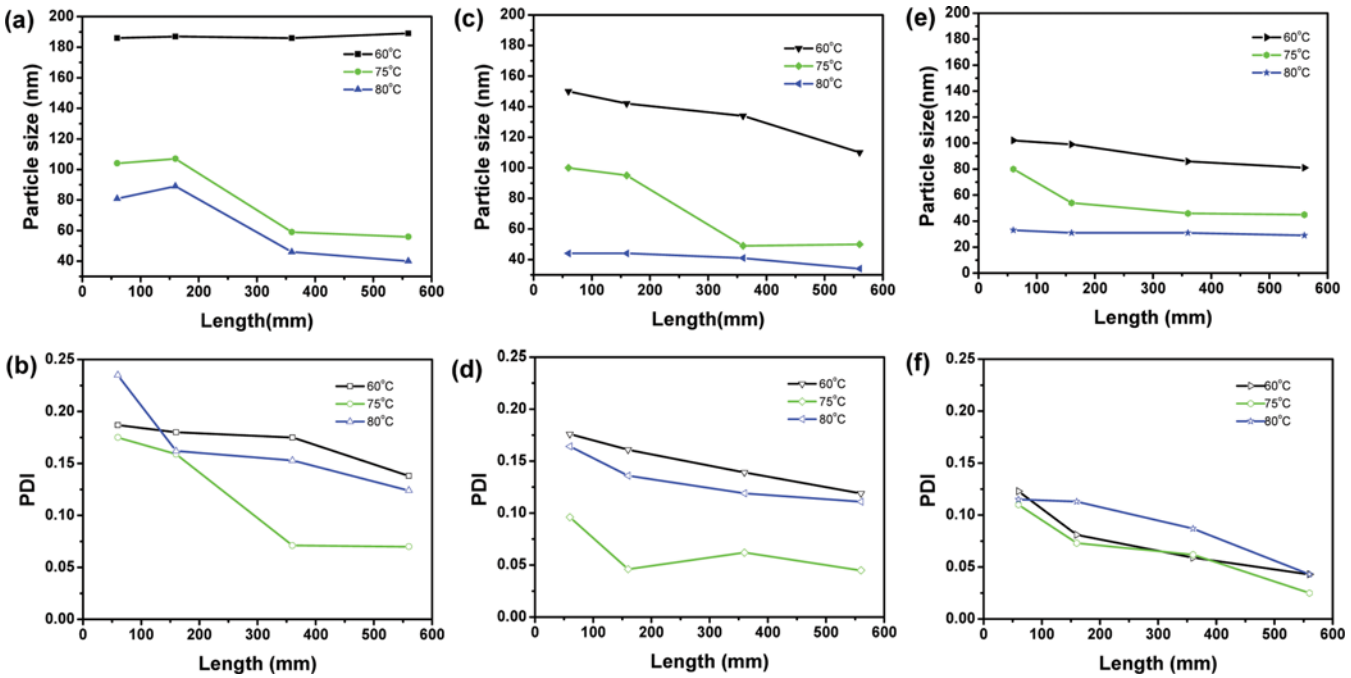

Fig. 7. Particle size and PDI value of silica obtained in the system with ID of (a) and (b) 1.5 mm; (c) and (d) 1.0 mm; (e) and (f) 0.68 mm. Reaction condition: C_{TEOS}=0.5 mol/L, C_{NH_4OH}=0.82 mol/L, C_{H_2O}=5.8 mol/L, T_{MX}=180°, time=1 h/2 h, V_A=V_B=0.038 m/s.

achieved by the smaller characteristic scale (l as seen in Eq. (4)). For example, the calculated Fo number (T=80 °C, L=60 mm) ranged from 0.09 to 0.45 as the microchannel diameter decreased from 1.5 mm to 0.68 mm. As mentioned, the increased mixing efficiency resulted in the decreased particle size.

Fig. 7(b), 7(d) and 7(f) present the effect of channel length and reaction temperature on the PDI value of silica nanoparticles with the channel diameter of 1.5 mm, 1.0 mm and 0.68 mm, respectively. As the channel length increased from 60 mm to 560 mm, the PDI value of silica obtained at the different temperature and in different channel diameter all decreased. As described above, the extended microchannel length resulted in a good mixing efficiency (the increased Fo number), which led to the uniform silica particles. In addition, the PDI value of silica synthesized in different microchannel diameter (while the reaction temperature and microchannel were the same) was in the order of 1.50 mm>1.00 mm>0.68 mm. The reason was that the decreased microchannel diameter resulted in a good mixing efficiency (the increased Fo number). The PDI value of silica nanoparticles obtained at 60 °C outweighed that at 75 °C, which agreed with the results of the batch reactor [17,21,59].

It can be concluded that the size and PDI value of silica nanoparticles synthesized in the microchannel decreased with channel length increasing or with the channel diameter decreasing. It can be found that the longer residence time (t) and smaller characteristic scale (l) resulted in better mixing efficiency, which was in accordance with the Eq. (4). The smaller reaction units gained by the better mixing efficiency in the microreactor led to more nuclei. Therefore, smaller silica particles were formed by the better mixing efficiency. The reaction temperature must also be taken under consideration together with the mixing efficiency. Because, the results of particle size and PDI value were both influenced by the organic combination of reaction rate and mixing efficiency. As discussed previously, the silica particles synthesized at low temperature had poor monodispersity due to the long nucleation phase. And then a better mixing efficiency (reduced diameter and increased length of microchannel) was needed at the lower temperature. For the slow reaction rate at low temperature, a long microchannel was required to achieve a good mixing efficiency. For example, as seen in Fig. 7(a), the particle size of silica synthesized at 60 °C remained unchanged even at the channel length of 560 mm. The particle size and PDI value remained unchanged at certain reaction temperature when it achieved a great mixing efficiency. As shown in Fig. 7(e), the particle size of silica synthesized at 80 °C remained almost unchanged as the channel length ranged from 60 mm to 560 mm.

6. Two-phase (Gas-liquid) Segmented Flow Reactor

As known in section 3.5, the uniformity of particles increased with the mixing efficiency increasing, which was attributed to uniform reaction condition of the reactants. In addition to the reduction of microchannel diameter and extension of microchannel length, an inert gas (nitrogen) was injected into the flow to cause a disturbance and promote the mixing efficiency. In this work, the influence of the mixing efficiency on the size and PDI value of silica nanoparticles was considered by changing the gas/liquid ratio (such as 1.7/1, 5/1 and 8.3/1). And the residence time remained the same by changing the microchannel length accordingly. The optical photographs of flow patterns with different gas-liquid ratios are presented in Fig. 8.

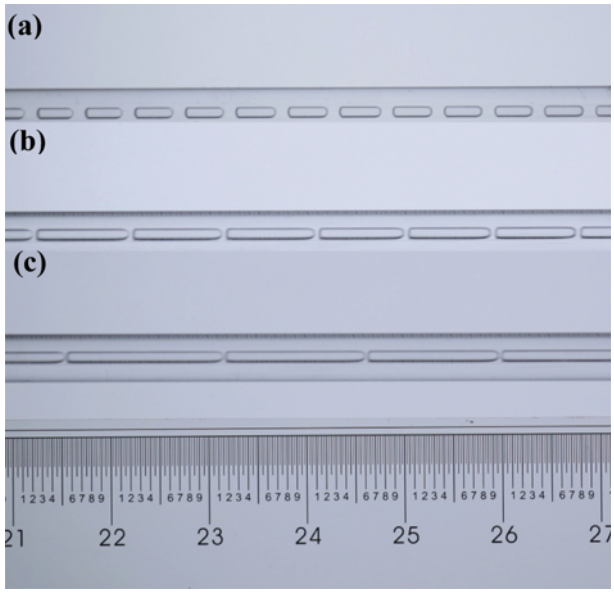

Fig. 8. Optical photographs of flow patterns with different gas (nitrogen)/liquid ratios: (a) 1.7/1; (b) 5/1; (c) 8.3/1. Reaction condition: C_{TEOS}=0.5 mol/L, C_{NH_4OH}=0.82 mol/L, C_{H_2O}=5.8 mol/L, ID=1.00 mm, T_{MX}=180°, V_A=V_B=0.038 m/s, time=1 h/2 h, temperature=60 °C.

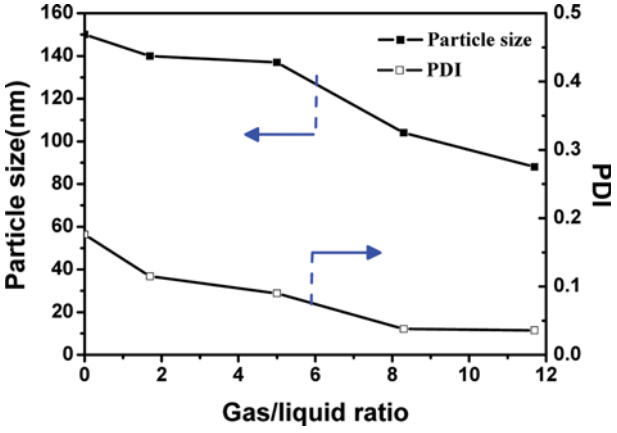

Fig. 9. Particle size and PDI value of silica prepared in the system with different gas (nitrogen)/liquid ratios: 0; 1.7/1; 5/1; 8.3/1. Reaction condition: C_{TEOS}=0.5 mol/L, C_{NH_4OH}=0.82 mol/L, C_{H_2O}=5.8 mol/L, ID=1.00 mm, T_{MX}=180°, V_A=V_B=0.038 m/s, time=1 h/2 h, temperature=60 °C.

Fig. 9 represents the effect of gas/liquid ratio on the size and PDI value of silica nanoparticles obtained in the microreactor with the channel diameter of 1.00 mm. Both the mean size and PDI value of silica nanoparticles obtained at the reaction temperature of 60 °C decreased with the gas/liquid ratio increasing. As seen in Fig. 8, the flow patterns in the microchannel were Taylor flow when the gas/liquid ratio increased from 1.7 to 8.3. In Taylor flow pattern, the mixing efficiency increases in the following two aspects: on one hand, the liquid-film thickness between the gas and the inner surface of the channel decreases, which minimizes the mixing

scale of the reactants in the solutions; on the other hand, the recirculation within the liquid slugs promotes the mixing of reactant in the liquid slugs [31]. At the large gas/liquid ratio, the short liquid slug between the gas slug and the long liquid film between the gas and surface of the channel led to the reduced characteristic scale of diffusion (l as seen in Eq. (4)). Thus, the increased Fo number resulted in a better mixing efficiency of the reactants. Then the silica particles with decreased size and narrow size distribution were obtained. As can be seen from Fig. 9, the high flow rate of gas resulted in a decreased particle size with high monodispersity in the microchannel. And it was in accordance with section 3.5 that the strong mixing led to uniform particles.

CONCLUSION

The poor mixing efficiency and local inhomogeneities in the batch reactor system resulted in silica nanoparticles with broad particle size distributions. And the long residence time (over 15 minutes [31]) in the microreactor for completing the reaction brings a long channel and high cost. To overcome disadvantages of the above systems, a combined micromixer/microreactor/batch reactor system was used to synthesize the silica nanoparticles. In the system, the microchannel intensified the mixing of the reactants, and the batch reactor supplied room for the growth and aging of silica nanoparticles. Compared with the batch reactor system, the silica nanoparticles with narrower particle size distributions, higher yields, and better sphericity were achieved in this work. The concentration of reactants and operation variables were controlled to synthesize the silica nanoparticles with different particle sizes (20 nm to 2 μm) and size distributions (0.01 to 0.4). Thus, it is possible to precisely control the particle size and size distributions of silica by varying those factors. To illustrate the relationship among mass transfer, mixing and reaction in the system, the silica particles with different sizes and monodispersities were synthesized by varying the reaction temperature, length and diameter of microchannel. The results showed that the smaller microchannel diameter and longer microchannel length caused a better mixing efficiency (higher Fo number), which led to the smaller particle size and higher monodispersity. In addition, inert gas was introduced into the microchannel to increase the mixing efficiency, which resulted in an even smaller particle size and narrower size distribution. Therefore, it was clearly demonstrated that high mixing efficiency resulted in decreased particle size with high monodispersity.

REFERENCES

1. M. Liong, B. France, K. A. Bradley and J. I. Zink, *Adv. Mater.*, **21**, 1684 (2009).
2. C. Yagüe, M. Moros, V. Grazú, M. Arruebo and J. Santamaría, *Chem. Eng. J.*, **137**, 45 (2008).
3. S. A. Johnson, P. J. Ollivier and T. E. Mallouk, *Science*, **283**, 963 (1999).
4. H. Yang and Y. Zhu, *Talanta*, **68**, 569 (2006).
5. C. J. S. Brinker, G. W., Sol-Gel Science: The Physics and Chemistry of Sol-Gel Processing, Academic Press (1990).
6. R. K. Iler, The Chemistry of Silica, Wiley (1979).
7. M. Su, H. J. Su, B. L. Du, X. T. Li, G. Y. Ren and S. D. Wang, *J. Sol-Gel. Sci. Technol.*, **73**, 460 (2015).
8. S. F. Wang, Y. F. Hsu, T. C. K. Yang, C. M. Chang, Y. Chen, C. Y. Huang and F. S. Yen, *Mater. Sci. Eng., A*, **395**, 148 (2005).
9. J. Z. Wang, A. Sugawara-Narutaki, M. Fukao, T. Yokoi, A. Shimojima and T. Okubo, *ACS Appl. Mater. Interfaces*, **3**, 1538 (2011).
10. F. Schüth, *Angew. Chem. Int. Ed.*, **42**, 3604 (2003).
11. C. Liang, Z. Li and S. Dai, *Angew. Chem. Int. Ed.*, **47**, 3696 (2008).
12. W. Stober, A. Fink and E. Bohn, *J. Colloid Interface Sci.*, **26**, 62 (1968).
13. S. K. Park, K. D. Kim and H. T. Kim, *Colloids Surf., A*, **197**, 7 (2002).
14. G. H. Bogush, M. A. Tracy and C. F. Zukoski, *J. Non-Cryst. Solids*, **104**, 95 (1988).
15. Z. Lei, Y. Xiao, L. Dang, M. Lu and W. You, *Micropor. Mesopor. Mater.*, **96**, 127 (2006).
16. R. Lindberg, J. Sjöblom and G. Sundholm, *Colloids Surf., A*, **99**, 79 (1995).
17. Y. Huang and J. E. Pemberton, *Colloids Surf., A*, **360**, 175 (2010).
18. F. J. Arriagada and K. Osseo-Asare, *J. Colloid Interface Sci.*, **211**, 210 (1999).
19. C. L. Chang and H. S. Fogler, *Langmuir*, **13**, 3295 (1997).
20. J. Esquena, T. F. Tadros, K. Kostarelos and C. Solans, *Langmuir*, **13**, 6400 (1997).
21. K. S. Finnie, J. R. Bartlett, C. J. A. Barbé and L. Kong, *Langmuir*, **23**, 3017 (2007).
22. F. Venditti, R. Angelico, G. Palazzo, G. Colafemmina, A. Ceglie and F. Lopez, *Langmuir*, **23**, 10063 (2007).
23. F. Asaro, A. Benedetti, I. Freris, P. Riello and N. Savko, *Langmuir*, **26**, 12917 (2010).
24. K. D. Hartlen, A. P. T. Athanasopoulos and V. Kitaev, *Langmuir*, **24**, 1714 (2008).
25. T. Yokoi, Y. Sakamoto, O. Terasaki, Y. Kubota, T. Okubo and T. Tatsumi, *J. Am. Chem. Soc.*, **128**, 13664 (2006).
26. T. M. Davis, M. A. Snyder, J. E. Krohn and M. T. Sapatsis, *Chem. Mater.*, **18**, 5814 (2006).
27. C. H. Chang, B. Paul, V. Remcho, S. Atre and J. Hutchison, *J. Nanopart. Res.*, **10**, 965 (2008).
28. E. H. Scott Fogl, Elements of Chemical Reaction Engineering, Prentice-Hall of India (2004).
29. K. D. Kim and H. T. Kim, *J. Sol-Gel Sci. Technol.*, **25**, 183 (2002).
30. P. He, G. Greenway and S. J. Haswell, *Chem. Eng. J.*, **167**, 694 (2011).
31. S. A. Khan, A. Gunther, M. A. Schmidt and K. F. Jensen, *Langmuir*, **20**, 8604 (2004).
32. L. Gutierrez, L. Gomez, S. Irusta, M. Arruebo and J. Santamaria, *Chem. Eng. J.*, **171**, 674 (2011).
33. M. Su, H. J. Su, B. L. Du, X. T. Li, G. Y. Ren and S. D. Wang, *J. Sol-Gel. Sci. Technol.*, **72**, 375 (2014).
34. M. Faryadi, M. Rahimi and M. Akbari, *Korean J. Chem. Eng.*, **33**, 922 (2016).
35. Y. Wakashima, A. Suzuki, S. Kawasaki, K. Matsui and Y. Hakuta, *J. Chem. Eng. Jpn.*, **40**, 622 (2007).
36. E. Lester, P. Blood, J. Denyer, D. Giddings, B. Azzopardi and M. Poliakoff, *J. Supercrit. Fluids*, **37**, 209 (2006).
37. K. Mae, A. Suzuki, T. Maki, Y. Hakuta, H. Sato and K. Arai, *J. Chem. Eng. Jpn.*, **40**, 1101 (2007).

38. S. Kawasaki, Y. Xiuyi, K. Sue, Y. Hakuta, A. Suzuki and K. Arai, *J. Supercrit. Fluids*, **50**, 276 (2009).
39. Y. Ying, G. Chen, Y. Zhao, S. Li and Q. Yuan, *Chem. Eng. J.*, **135**, 209 (2008).
40. Y. Huang and J. E. Pemberton, *Colloids Surf., A*, **377**, 76 (2011).
41. K. Nozawa, H. Gailhanou, L. Raison, P. Panizza, H. Ushiki, E. Sellier, J. P. Delville and M. H. Delville, *Langmuir*, **21**, 1516 (2005).
42. T. Matsoukas and E. Gulari, *J. Colloid Interface Sci.*, **124**, 252 (1988).
43. G. H. Bogush and C. F. Zukoski, *J. Colloid Interface Sci.*, **142**, 1 (1991).
44. W. G. Klemperer and S. D. Ramamurthi, *J. Non-Cryst. Solids*, **121**, 16 (1990).
45. H. Boukari, J. S. Lin and M. T. Harris, *J. Colloid Interface Sci.*, **194**, 311 (1997).
46. K. Lee, J. L. Look, M. T. Harris and A. V. McCormick, *J. Colloid Interface Sci.*, **194**, 78 (1997).
47. J. Park, J. Joo, S. G. Kwon, Y. Jang and T. Hyeon, *Angew. Chem. Int. Ed.*, **46**, 4630 (2007).
48. D. L. Green, S. Jayasundara, Y. F. Lam and M. T. Harris, *J. Non-Cryst. Solids*, **315**, 166 (2003).
49. V. K. LaMer and R. H. Dinegar, *J. Am. Chem. Soc.*, **72**, 4847 (1950).
50. J. Guo, X. Lu, Y. Cheng, Y. Li, G. Xu and P. Cui, *J. Colloid Interface Sci.*, **326**, 138 (2008).
51. D. C. L. Vasconcelos, W. R. Campos, V. Vasconcelos and W. L. Vasconcelos, *Mater. Sci. Eng., A*, **334**, 53 (2002).
52. R. Watanabe, T. Yokoi, E. Kobayashi, Y. Otsuka, A. Shimojima, T. Okubo and T. Tatsumi, *J. Colloid Interface Sci.*, **360**, 1 (2011).
53. A. V. Blaaderen, J. V. Geest and A. Vrij, *J. Colloid Interface Sci.*, **154**, 481 (1992).
54. S. M. Chang, M. Lee and W. S. Kim, *J. Colloid Interface Sci.*, **286**, 536 (2005).
55. J. R. Burns and C. Ramshaw, *Chem. Eng. Res. Des.*, **77**, 206 (1999).
56. J. Crank, The Mathematics of Diffusion, Oxford Science Publications (1979).
57. G. S. Laddha and T. E. Degaleesan, Transport Phenomena in Liquid Extraction, McGraw-Hill, New York (1978).
58. D. F. Othmer and H. T. Chen, *Ind. Eng. Chem. Proc. Des. Develop.*, **1**, 249 (1962).
59. I. A. Rahman, P. Vejayakumaran, C. S. Sipaut, J. Ismail, M. A. Bakar, R. Adnan and C. K. Chee, *Colloids Surf., A*, **294**, 102 (2007).